

Jet-cloud interactions and the brightening of the narrow line region in Seyfert galaxies

W. Steffen¹, J.L. Gómez², A.C. Raga³ and R.J.R. Williams⁴

ABSTRACT

We study the kinematical and brightness evolution of emission line clouds in the narrow line region (NLR) of Seyfert galaxies during the passage of a jet. We derive a critical density above which a cloud remains radiative after compression by the jet cocoon. The critical density depends mainly on the cocoon pressure. Super-critical clouds increase in emission line brightness, while sub-critical clouds generally are highly overheated reducing their luminosity below that of the inter-cloud medium.

Due to the pressure stratification in the bow-shock of the jet, a cylindrical structure of nested shells develops around the jet. The most compact and brightest compressed clouds surround the cloud-free channel of the radio jet. To support our analytical model we present a numerical simulation of a supersonic jet propagating into a clumpy NLR. The position-velocity diagram of the simulated H α emission shows total line widths of the order of 500 km s⁻¹ with large-scale variations in the radial velocities of the clouds due to the stratified pressure in the bow-shock region of the jet. Most of the luminosity is concentrated in a few dense clouds surrounding the jet. These morphological and kinematic signatures are all found in the well observed NLR of NGC 1068 and other Seyfert galaxies.

Subject headings: galaxies: active - galaxies: jets - galaxies: kinematics and dynamics - galaxies: Seyfert - methods: numerical - hydrodynamics - shock waves

¹Department of Physics and Astronomy, University of Manchester, Manchester M13 9PL, UK; wsteffen@ast.man.ac.uk

²Instituto de Astrofísica de Andalucía, CSIC, Apdo. 3004, Granada 18080, Spain; jlgomez@iaa.es

³Instituto de Astronomía, UNAM, Apdo. Postal 70-264, 04510 México, D.F., Mexico; raga@astroscu.unam.mx

⁴Department of Physics and Astronomy, The University, Leeds LS2 9JT, UK; rjr@ast.leeds.ac.uk

1. Introduction

Distinct signs of interaction between a collimated radio jet and a clumpy narrow line region (NLR) are found in some Seyfert galaxies (e.g. NGC 1068), such as morphological association between radio and optical structures (Capetti et al. 1995, Capetti, Macchetto, & Lattanzi 1997; Gallimore, Baum, & O’Dea 1996) and/or in wide spectral lines of FWHM $\sim 1000 \text{ km s}^{-1}$ (Veilleux 1991). Even though ground-based spatially resolved spectroscopy has yielded some information on the kinematics of individual clouds and the relation to the interaction with the radio outflows (Wagner & Dietrich 1996; Pécontal et al. 1997) it is not yet clear whether the high velocities of the clouds can be attributed to the interaction with the jet. The new Space Telescope Imaging Spectrograph (STIS) on the Hubble Space Telescope (HST) should provide the necessary spatial resolution to test this jet-cloud interaction hypothesis.

Apart from the kinematics we consider the structural changes in the NLR caused by the interaction with a jet. Linked to this question is whether the interaction increases or decreases the overall emission line luminosity, making it more or less likely to observe a jet-NLR association as compared to an undisturbed NLR. We consider the fate of clouds with varying density and size after the interaction with the jet cocoon. This problem is similar to the case of a supernova shock over-running a cloud in the interstellar medium which has been studied by several authors (e.g. McKee & Cowie 1975; Hartquist & Dyson 1993 and references therein; Klein, McKee, & Colella 1994). The adiabatic interaction of a jet with an ensemble of clouds has been studied numerically by Higgins, O’Brien, & Dunlop (1995). Bicknell, Dopita, & O’Dea (1997) have presented an analytical approach to explain the relationship between emission-line luminosity and radio-power in different classes of AGN using a model based on the jet/cocoon interaction with the ISM. Steffen et al. (1997b) have carried out non-adiabatic simulations of a jet propagating into a filamentary medium on the scale of the NLR in Seyfert galaxies.

In this Letter we concentrate on the consequences of the interaction on a large ensemble of clouds based on analytic and numerical calculations of the change of the luminosity of the clouds. In particular, we discuss the effect which the stratification of pressure in the bowshock has on the kinematics and emission of the ensemble of clouds.

2. Critical cloud densities

In this section we derive a minimum number density n_{cc} for a cloud above which radiative shock compression occurs after being entrained or hit by the over-pressured cocoon of the jet.

If the compressing shock is radiative, the luminosity increases, while otherwise the cloud is overheated and reduces its emission line brightness. In order to derive the critical density we assess whether the cooling time t_{cool} of a compressed cloud of initial density n_{c0} is sufficiently small to lead to a dense, cold cloud with a temperature T_{cf} similar to its initial value T_{c0} ($\approx 10^4\text{K}$) within a shock crossing time t_{cc} . Hence, we require $t_{\text{cool}} < t_{\text{cc}}$.

In order to compare the shock crossing time with the cooling time we assume a cooling function of the form $\Lambda(T) = \Lambda_0 T^{-\alpha}$ (with $\Lambda_0 = 4.6 \times 10^{-18} \text{erg s}^{-1} \text{cm}^3$ and $\alpha = 0.76$ for $T > 1.5 \times 10^5 \text{K}$; Taylor, Dyson, & Axon 1992), where T is the temperature. The cooling of the immediate post-shock gas can then be expressed in terms of the pressure P driving the shock, using $T = P/\sigma n_{c0} k$ (where $\sigma = 4$ is the compression ratio by a strong adiabatic shock and k is the Boltzmann constant):

$$\Lambda(P) = \Lambda_0 \left(\frac{P}{\sigma n_{c0} k} \right)^{-\alpha}. \quad (1)$$

The cooling time-scale t_{cool} of the post-shock gas is given by the ratio between the internal energy γP and the cooling rate $(\sigma n_{c0})^2 \Lambda(P)$,

$$t_{\text{cool}} = \frac{\gamma P^{1+\alpha}}{k^\alpha (\sigma n_{c0})^{2+\alpha} \Lambda_0} \quad (2)$$

where we made use of equation (1) and $\gamma = 5/3$ is the specific heat ratio for a monatomic gas. The critical density n_{cc} of a cloud above which it will cool sufficiently fast to the photoionization equilibrium temperature is estimated by equating the cooling time with the time $t_{\text{cc}} = d_{c0} v_c^{-1}$ which the compressing shock of speed v_c takes to cross a cloud of size d_{c0} . The propagation speed of the shock in a cloud of number density n_{c0} can be calculated using

$$v_c = \left(\frac{\xi P}{\mu n_{c0}} \right)^{\frac{1}{2}}, \quad (3)$$

where μ is the average mass per atom or ion and $\xi = 1$ for a strong isothermal shock and $\xi = 4/3$ otherwise.

Combining equations (2) and (3) with the shock crossing time we find the critical number density n_{cc} of the unshocked cloud as a function of the compressing pressure and initial cloud size

$$n_{\text{cc}} = \left(\frac{\xi^{1/2} \gamma P^{3/2+\alpha}}{\sigma^{2+\alpha} k^\alpha \Lambda_0 \mu^{1/2} d_{c0}} \right)^{\frac{1}{\alpha+5/2}}. \quad (4)$$

The fact that there is a critical density for the brightening of a cloud, which depends mainly on the pressure in the cocoon, has important consequences which could be used to test the significance of the jet for the observed structure of the NLR. Note that the cocoon pressure

(including ram-pressure) near the head of the bow-shock of the jet gradually decreases from the axis outwards and from the head towards the source of the jet, until it reaches a roughly constant value. Therefore the critical density for the clouds to survive the passage of the cocoon shock decreases with distance from the jet axis. Consequently, low-density clouds and filaments will not survive near the jet axis, resulting in an cylindrical stratification of clouds of different compression around the jet. This structure is illustrated in the schematic diagram of Figure 1 which shows the inferred stratification as seen along the jet axis. If a cloud is inhomogeneous, the sub-critical envelope will be stripped off leaving only any super-critical core. The compactness of the clouds increases towards the axis, but no clouds will be found at least over a full jet radius.

3. Luminosity change of shocked NLR clouds

We now estimate the brightening of a super-critical cloud ($n_{c0} > n_{cc}$) with uniform densities n_{c0} and n_{cf} before and after the compression, respectively. The luminosity ratio is then

$$\frac{L_{cf}}{L_{c0}} = \frac{\epsilon_{cf} V_{cf}}{\epsilon_{c0} V_{c0}} \quad (5)$$

where $\epsilon \propto n^2$ and V are the volume emissivity and the volume of the cloud, respectively. Using the assumption that no mass M ($V = M/n$) is lost during the compression (e.g. by ablation or fragmentation), we obtain from the previous equation

$$\frac{L_{cf}}{L_{c0}} = \frac{n_{cf}}{n_{c0}}. \quad (6)$$

The final compression ratio n_{cf}/n_{c0} can be determined independently considering that the final pressure of the cloud is the same as the cocoon pressure P driving the shock into the cloud. Using $P = n_{cf} k T_{cf}$ and $T_{cf} \approx T_{c0}$ together with equation (6) we find a very simple expression for the final luminosity ratio in terms of the pressure of the cloud before and after the compression

$$\frac{L_{cf}}{L_{c0}} = \frac{P}{n_{c0} k T_{cf}} = \frac{P}{P_{c0}} \quad (7)$$

where P_{c0} is the initial pressure of the cloud. The luminosity increase of the shocked gas in a super-critical cloud as compared to its undisturbed value varies as the change in pressure which it experiences. In the presence of magnetic fields, the compression might be limited by the magnetic pressure of the compressed cloud rather than the thermal pressure at the photoionization equilibrium temperature. If the cloud is too large to be fully processed in the time-scale of the jet propagation, the increase in brightness will of course apply only to the shocked fraction of the cloud. If the final density is above the critical density for collisional

deexcitation, the emissivity is no longer proportional to n^2 and the increase in luminosity is different to the one predicted by our simple model, which nevertheless predicts the correct qualitative result.

A similar calculation for an adiabatic shock yields the luminosity ratio for a sub-critical cloud before and after compression

$$\frac{L_{\text{uf}}}{L_{\text{u0}}} = \sigma^{\frac{5}{2}} \left(\frac{P}{P_{\text{c0}}} \right)^{-\frac{3}{2}} \quad (8)$$

Here we used equations (5) and (6) with compression ratio σ and volume emissivity $\epsilon \propto n^2 T^{-3/2}$. The scaling of the emissivity with temperature follows the dependence of the recombination coefficient. The initial and final temperatures are assumed to be $T_{\text{c0}} = P_0/kn_{\text{c0}}$ and $T_{\text{cf}} = P/k\sigma n_{\text{c0}}$. Equation (8) shows that the sub-critical clouds generally lose flux, since the pressure ratio can be expected to be much higher than the compression ratio. Moreover, one finds that their specific emissivity falls below that of the environment ϵ_{x} , in which they where embedded, by a factor of

$$\frac{\epsilon_{\text{uf}}}{\epsilon_{\text{x}}} = \sigma^{\frac{7}{2}} \left(\frac{P}{P_{\text{c0}}} \right)^{-\frac{3}{2}} \quad (9)$$

This basically renders the sub-critical clouds invisible in emission lines which are emitted most strongly near the equilibrium temperature. Even though the cooling time of the hot clouds is much larger than the internal shock crossing time, it may be of order of the jet propagation time through the NLR ($10^{12} - 10^{14}$ sec). Consequently these clouds may start radiating after a time of this order of magnitude and produce emission lines radiated at temperatures higher than the equilibrium temperature near 10^4 K with relatively large velocities. Even though in our numerical simulation (see below) the emission measure of the hot gas (3×10^4 to 3×10^5 K) is found to be very low compared to that at lower temperatures (5000 to 30000 K) (ratio = 1/530), this emission, together with the observed radio emission, could serve as an indicator of the propagation time of the jet, displaying a variation of temperature and hence the excitation of the clouds as a function of distance from the central AGN.

If the NLR is made purely of sub-critical gas, the jet will plough a cylindrical hole into it. However, if there is a sufficiently large number of super-critical clouds present, a region of increased emission line brightness will trace the cocoon of the jet. If the average density of the NLR clouds falls with distance from the centre, there will be a rather sharp transition region beyond which the clouds are all sub-critical. The consequence will be that the number of strong shocked NLR clouds will sharply decrease in this region, even if the jet has already propagated further out, as is observed, e.g. in NGC4151 (Boksenberg et al. 1995; Pedlar et al. 1993) and NGC 1068 (Gallimore et al. 1996).

For the NLR to increase in total luminosity due to the passage of the jet, the ratio

between the mass M_{c0} concentrated in super-critical clouds of uniform density n_{c0} and the mass M_{u0} of sub-critical clouds of uniform density n_{u0} does not need to be very large, but approximately only

$$\frac{M_{c0}}{M_{u0}} > \frac{P_{c0}}{P} \left(\frac{n_{u0}}{n_{c0}} \right)^{9/2}. \quad (10)$$

Equation (10) shows that the change in overall luminosity of the NLR depends strongly on the initial average density and mass of the affected clouds. Only if the total mass of sub-critical clouds is much larger than the mass of the super-critical ones, can the total luminosity be comparable for both ensembles. They could contribute noticeably to the low brightness, but fast wings observed in the emission lines of many Seyferts. Most of the luminosity though is likely to be concentrated in a few dense clouds relatively near the jet axis following the galactic rotation with disturbances of the order of 100-300 km s⁻¹. This is largely consistent with observations of NGC 1068 (Wagner & Dietrich 1996) and NGC 4151 (Winge et al. 1997).

If initially neutral material is overrun by the cocoon, the increase in volume emissivity of the shocked material can be expected to be much larger than the one predicted to occur in preionized clouds, since the neutral clouds do not emit appreciably in forbidden lines. They might well be at least partially pre-ionized by the radiation coming from the cocoon shock (e.g. Bicknell, Dopita, & O’Dea 1997), leading to two qualitatively different stages of increase in brightness, the first being due to precursor photo-ionization and the second due to ionization and compression by the cocoon shock. Consequently, in a statistical sample of Seyfert galaxies, positional associations between radio jets and emission line gas could be biased towards galaxies with more neutral gas in the region of interaction.

Other expected observable consequences of the stratified structure include a radial variation of the cloud kinematics (faster near the jet axis) and of the ionization properties of the clouds (since the column density of neutral ions in the clouds increases due to the higher recombination rate in the compressed clouds). Possibly, even polarization properties of scattered nuclear radiation through the compression of seed magnetic fields might be observable, since the ram-pressure in the bow-shock will produce enhanced compression perpendicular to the surface of the bow-shock.

4. Numerical simulation

In order to test our analytical model we carried out two-dimensional numerical hydrodynamic simulations in slab-geometry with the code described in Raga et al. (1995) and Steffen et al. (1997a). The code uses the flux-vector slitting scheme by van Leer (1982) on

a 5-level binary adaptive grid. Initially the NLR is stationary and is assumed fully ionised throughout. The intercloud medium (ICM) of the NLR has a number density of 1 cm^{-3} and a pressure of $2 \times 10^{-12} \text{ dyn cm}^{-2}$. The spherical NLR clouds have random positions, radii in the range $0.5 - 1.5 \times 10^{19} \text{ cm}$ and a number density of up to 500 cm^{-3} (cloud pressure of $1.4 \times 10^{-9} \text{ dyne cm}^{-2}$ for $n = 500$). Most of the mass is concentrated in the clouds (mass ratio between clouds and ICM is 8.7). The jet has a velocity of $6 \times 10^9 \text{ cm s}^{-1}$, a number density of 0.3 cm^{-3} , and a radius of $8 \times 10^{18} \text{ cm}$. The cooling is treated as described in Steffen et al. (1997a), with a lower limit set to 10^4 K to simulate photoionization equilibrium (ionization presumably from a the nuclear radiation source). The grid size is 513^2 cells or $(10^{21} \text{ cm})^2$.

The results from the simulation are shown in Figure 2, where greyscale images show the distributions of density (A), the $\text{H}\alpha$ emissivity (B), the initial density (C) and the position-velocity diagrams (D) of the $\text{H}\alpha$ emissivity as seen from directions along (0°) and perpendicular (90°) to the axis of the jet. Figure 3 shows the integrated $\text{H}\alpha$ spectrum. Panel (B) also shows a contour of high temperature ($3 \times 10^9 \text{ K}$) indicating the region where the jet plasma is located and hence from where any radio emission can be expected to originate, even though the temperature cannot be a direct measure for the radio intensity. For a short time the jet was bent towards the top-right corner, while in the image shown, it bends slightly downwards.

The jet propagates into the inhomogeneous NLR shocking the clouds and the ICM over a large area with a roughly uniform cocoon pressure. The clouds are entrained into the cocoon and compressed in the way discussed in Section 2. Note that in a fully three-dimensional simulation, the transvers extent of the pressurized region would be somewhat smaller than in this slab-symmetric simulation. The clouds marked with open arrows in Panel C are sub-critical clouds and are destroyed during compression by the cocoon pressure (see same positions marked in Panel A). The other clouds are super-critical and turn into discrete, strongly compressed density concentrations at or near the original position. There are, however, a number of exceptions, which we have marked with filled arrows. These clouds are super-critical to the cocoon pressure, but were located either directly in the path of the jet or close to the jet axis, where the pressure (and therefore the critical density) was higher when the interaction started, leading to the destruction of the clouds.

The compactness and brightness of the surviving clouds increases towards the path of the jet. The increased brightness near the jet can be seen in Panel B, where the $\text{H}\alpha$ emission is shown convolved with a gaussian of FWHM of 10 pc. Here we marked three zones. First, a zone of fully processed compact clouds of highest brightness (a). This region is surrounded by zone (b) where clouds are less bright and compact or have been only partially processed

(see Panel A), while clouds in the outer zone (c) have only started the interaction or are still untouched by the jet cocoon showing very low brightness. This cylindrical shell structure resembles very much the one observed in NGC 1068 (Capetti et al. 1997) and NGC 4151 (Winge et al. 1997). The objects show zones of avoidance of NLR clouds, coincident with radio features, surrounded by high brightness clouds and weaker filamentary emission further out.

Compared to the initial conditions, we find that the peak emissivity rose by approximately three orders of magnitude, strongly emphasizing a few very dense clouds which emit most of the emission (see the total spectrum in Figure 3). The kinematical disturbance caused by the passage of the jet through the NLR is most pronounced near the head of the jet. Most of the strongly emitting gas moves at velocities under 300 km s^{-1} , producing a linewidth of around 600 km s^{-1} , enhanced by galactic rotation or initial turbulence, which have not been taken into account in this simulation. Some cloud material with low emissivity however has been accelerated to speeds of 500 km s^{-1} and higher. Seen along a line of sight perpendicular to the jet (Panel D, 90°), the pv-diagram appears symmetric. Here the amount of gas approaching and receding from the observer is well balanced, since the clouds are compressed equally from all sides without much acceleration perpendicular to the jet. Viewed along the axis of the jet (Panel D, 0°) the acceleration of the clouds due to the interaction with the bowshock shows as a positive velocity centroid of the cloud emission (see also Figure 3). There is a gradient of increasing velocity of the clouds towards the axis of the jet, consistent with expectations from the stratified accelerating (ram-)pressure in the bow-shock region.

The morphological and kinematical characteristics of our model are very similar to those observed in NGC 1068 (e.g. Capetti et al. 1997; Wagner & Dietrich 1996) and other NLR of Seyfert galaxies with associated radio jets and we suggest that the entrainment and compression of NLR clouds by the stratified cocoon pressure of a supersonic jet is the mechanism dominating the brightness and kinematics of the NLR in this galaxy. Spectral observations with high spatial resolution, like those of NGC 1068 presented by Pécontal et al. (1997) or of NGC 4151 using HST by Winge et al. (1997), will soon provide sufficient data to test the general applicability of our model, searching for the predicted stratified kinematic and structural signatures of the jet-NLR interaction.

5. Acknowledgements

WS acknowledges a PPARC research associateship and is grateful for the hospitality received by members of the Instituto de Astrofísica de Andalucía during which part of this

research was done. RJRW acknowledges a PPARC advanced fellowship. This research was partially supported by Spanish DGICYT (PB94-1275).

REFERENCES

- Bicknell, G.V., Dopita, M.A., O’Dea, C.P.O. 1997, *ApJ*, 485, 112
- Boksenberg, A., Catchpole, R.M., Macchetto, F., et al. 1995, *ApJ*, 440, 151
- Capetti, A., Axon, D.J., Kukula, M., Macchetto, F., Pedlar, A., Sparks, W.B., Boksenberg, A. 1995, *ApJ*, 454, L85
- Capetti, A., Macchetto, F.D., Lattanzi, M.G. 1997, in “Proceedings of the NGC 1068 Workshop”, eds. J.F. Gallimore and L.J. Tacconi, *Ap&SS*, in press
- Gallimore, J.F., Baum, S.A., O’Dea, C.P. 1996, *ApJ*, 464, 198
- Hartquist, T.W., Dyson, J.E. 1993, *QJRAS*, 34, 57
- Higgins, S., O’Brien, T.J., Dunlop, J. 1995, *Ap&SS*, 233, 311
- Klein, R.I., McKee, C.F., Colella, P. 1994, *ApJ*, 420, 213
- McKee, C.F., Cowie, L.L. 1975, *ApJ*, 195, 715
- Pécontal, E., Ferruit, P., Binette, L., Wilson, A.S. 1997, in “Proceedings of the NGC 1068 Workshop”, eds. J.F. Gallimore and L.J. Tacconi, *Ap&SS*, in press
- Pedlar, A., Kukula, M.J., Longley, D.P.T., Muxlow, T.W.B., Axon, D.J., Baum, S., O’Dea, C.O., Unger, S.W. 1993, *MNRAS*, 263, 471
- Raga, A.C., Taylor, S.D., Cabrit, S., Biro, S. 1995, *A&A*, 296, 833
- Steffen W., Gómez J.L., Williams R.J.R., Raga A.C., Pedlar A., 1997a, *MNRAS*, 286, 1032.
- Steffen, W., Pedlar, A., Gómez, J.L., Raga, A.C. 1997b, in “Proceedings of the NGC 1068 Workshop”, eds. J.F. Gallimore and L.J. Tacconi, *Ap&SS*, in press
- Taylor, D., Dyson, J.E., Axon, D.J. 1992, *MNRAS*, 255, 351
- van Leer, B. 1982, *Lect. Notes in Physics*, 170, 507
- Veilleux, S. 1991 *ApJS*, 75, 357

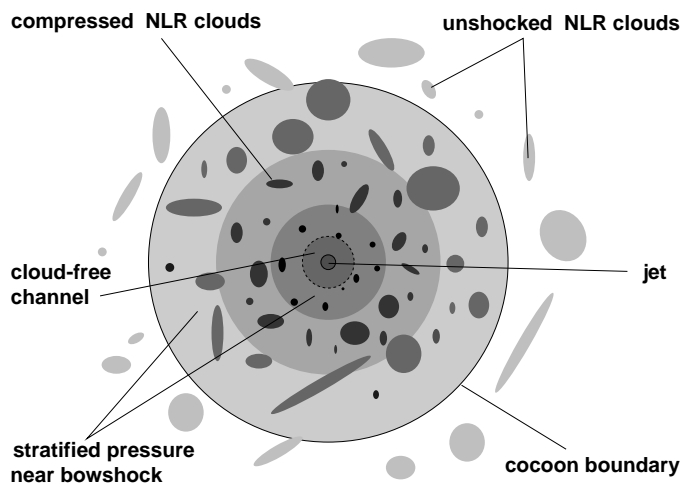
Wagner, S.J., Dietrich, M. 1996, 'NLR Kinematics of NGC 1068', in 'Science with the Hubble Space Telescope – II', P. Benvenuti, F. D. Macchetto, and E. J. Schreier (eds.),

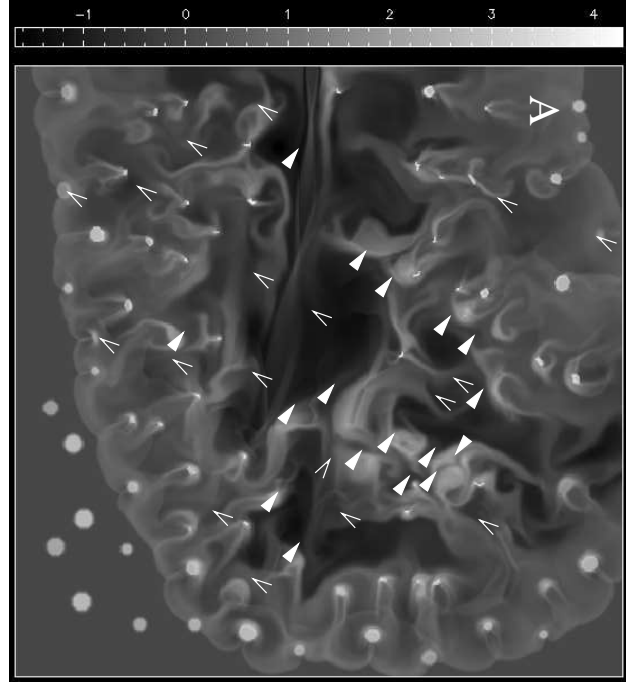
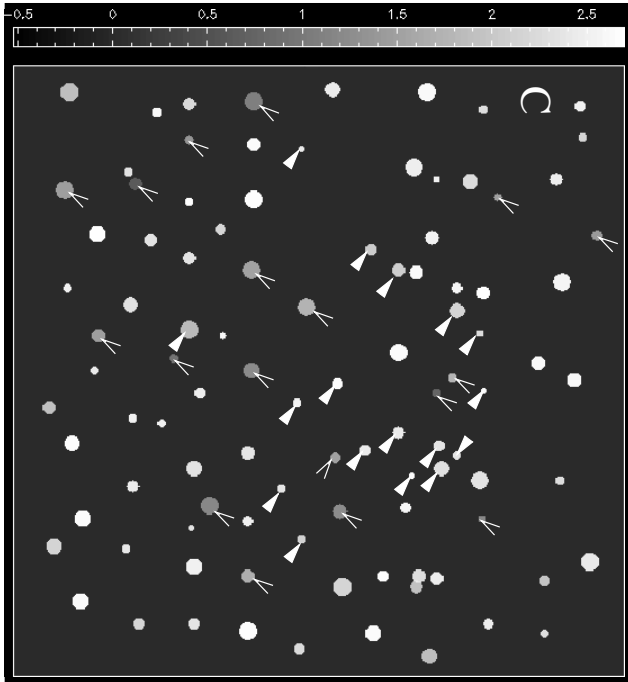
Winge, C., Axon, D.J., Macchetto, F.D., Capetti, A. 1997, ApJ, in press

Fig. 1.— A schematic view of the radial stratification of clouds after the entrainment by the cocoon of a supersonic extragalactic jet as seen along the jet axis. The compactness of the surviving clouds decreases with increasing distance from the jet axis.

Fig. 2.— Greyscale distributions are shown for the final density (A, logscale), the H α emissivity and temperature contours (B, linear scale), the initial number density (C, logscale) and the H α position-velocity diagrams (D, rooted greyscale and contours) as seen from directions along (0°) and perpendicular (90°) to the axis of the jet. In the top pv-diagram positions along the jet axis are aligned with those in Panel B. For easier comparison with observations, the H α -emissivity map and the pv-diagrams have been convolved with a Gaussian point-spread-function of FWHM of 10 pc and 60 km s $^{-1}$ in space and velocity, respectively.

Fig. 3.— The integrated H α line profiles for viewing angles which are aligned (0°) and perpendicular (90°) to the jet axis. The peak at zero-velocity is mainly due to undisturbed gas.





velocity [km/s]

